

RadOT-Eval: Auditable Structured-Evidence Transport for Radiology Report Evaluation

Weixin Liu¹, Juming Xiong¹, Yang Li¹, Qingyuan Song¹,
Susannah Rose², Murat Kantarcioglu³, Bradley Malin^{1,2}, Zhijun Yin^{1,2}

¹Vanderbilt University, Nashville, TN, USA

²Vanderbilt University Medical Center, Nashville, TN, USA

³Virginia Tech, Blacksburg, VA, USA

Email: {weixin.liu, juming.xiong, yang.li.2, qingyuan.song}@vanderbilt.edu,
muratk@vt.edu, {susannah.rose, b.malin, zhijun.yin}@vumc.org

Abstract—Automatic evaluation is critical for high-stakes text generation, where errors often involve omitted findings, hallucinated content, polarity reversals, location changes, uncertainty mismatches, and temporal-comparison errors rather than low surface similarity alone. Radiology report generation provides a challenging test case because generated reports must preserve structured clinical evidence across sources. We present RadOT-Eval, an interpretable structured-evidence optimal transport framework for offline auditing of radiology report generation. RadOT-Eval decomposes reference and candidate reports into attribute-structured clinical evidence units, aligns corresponding evidence using entropy-regularized optimal transport, and uses clinically meaningful side-channel discrepancies in a monotone risk model to predict error burden. All transport, feature, and readout choices are selected using the ReXVal dataset, and the frozen system is evaluated on the independent RadEvalX dataset. RadOT-Eval achieves Spearman correlations of 0.715, 0.548, and 0.399 with total, clinically significant, and clinically insignificant annotated error burden, respectively, yielding higher point estimates than standard evaluation metrics and the open-source large language model (LLM)-based evaluator GREEN-radllama2-7B. In a frozen auxiliary corruption-sensitivity stress test on ReXErr-v1, RadOT-Eval achieves 0.768 AUROC and a 0.990 corrupted-greater-than-clean paired win rate. These results show that structured evidence transport provides an auditable, rank-oriented evaluation tool for high-stakes generated clinical text under ReXVal-only model selection and frozen RadEvalX testing.

Index Terms—health informatics, radiology report evaluation, high-stakes text generation, optimal transport, interpretable model auditing

I. INTRODUCTION

Automatic evaluation is a central problem for generated-text systems because surface overlap can miss factual inconsistency, unsupported content, and omissions [1]–[3]. This issue is especially important in high-stakes domains, where generated documents must preserve local facts, negation, uncertainty, temporal context, and domain-specific risk. Radiology report generation is a representative setting because AI-generated reports may omit clinically important findings, hallucinate unsupported findings, reverse polarity, change anatomy or laterality, or misstate comparison with a prior study [4]–[7]. Such errors can be clinically significant even when the candidate report has a high lexical or semantic overlap with the reference report [8]–[11].

Existing radiology report evaluation metrics leave a gap for auditable discrepancy prediction that can be assessed without tuning on the final evaluation benchmark. Lexical, learned, and embedding-based metrics provide useful global similarity signals, but they do not expose which clinical statements were aligned or which local attributes disagreed [8], [9], [12]–[15]. While clinical label- and graph-based metrics such as CheXbert, RadGraph, RadGraph-XL, and RadCliQ incorporate domain structure, they could still obscure the local evidence behind a score [7], [16]–[18]. Large language model (LLM)-based and radiology-specific evaluators such as GREEN-radllama2-7B and RaTEScore can produce clinically oriented judgments or relevance scores. However, their outputs are not easily decomposed into stable local alignment decisions [19], [20]. This limitation is especially important for cross-source evaluation, where expert-annotated radiology benchmarks are typically small. Methods that require target-set tuning after inspecting target performance may overfit to the evaluation set rather than measure true generalization.

In this paper, we address this gap with RadOT-Eval (Fig. 1), which formulates radiology report evaluation as structured clinical evidence transport. This formulation is motivated by the fact that corresponding clinical findings may differ in wording, ordering, and granularity, while clinically important errors often arise from localized changes in polarity, anatomy, uncertainty, severity, devices, or temporal comparison. RadOT-Eval decomposes each reference and candidate report into attribute-structured clinical units capturing findings, anatomy, polarity, uncertainty, comparison, device, modifier, severity, and supporting text. OT then aligns these units using relatively stable clinical anchors, including finding identity, anatomy, polarity, and lexical evidence. Unlike prior OT-based text metrics that transport over words or contextual token embeddings, RadOT-Eval transports over extracted clinical evidence units and separates evidence alignment from clinical risk readout. Under the learned transport plan, variation-sensitive attributes are measured as side-channel discrepancies. A monotone nonnegative readout combines OT-based alignment evidence and discrepancy signals into ranked risk scores for total, clinically significant, and clinically insignificant errors. This design yields rank-oriented risk scores and inspectable aligned

evidence pairs, supporting offline model-development audit before prospective clinical evaluation.

We select transport, feature, and readout choices on the Radiology Report Expert Evaluation (ReXVal) dataset [21] and evaluate the frozen system on the independent Radiology Report Generation Models Evaluation Dataset for Chest X-rays (RadEvalX) [11]. RadOT-Eval reaches Spearman correlations of 0.715, 0.548, and 0.399 with total, clinically significant, and clinically insignificant error burden, yielding higher point estimates than the official RadEvalX standard metric baselines and the open-source LLM-based evaluator GREEN-radllama2-7B. On the auxiliary synthetic-error benchmark ReXErr-v1 [22], [23], the frozen system achieves 0.768 AUROC and a 0.990 corrupted-greater-than-clean paired win rate. Ablations, shortcut controls, and robustness diagnostics show that high-severity errors are driven primarily by structured clinical discrepancies, whereas low-severity errors are more affected by report complexity. These analyses position RadOT-Eval as an applied, auditable evaluator for model-development workflows rather than a replacement for radiologist review.

II. RELATED WORK

A. Structured evaluation of generated text

Automatic text-generation evaluation has moved beyond surface overlap toward semantic, factual, and task-specific assessment. Lexical and consensus metrics such as BLEU, ROUGE, METEOR, CIDEr, and SPICE provide useful corpus-level similarity signals, but they do not directly verify local facts, negation, uncertainty, or temporal context [8], [9], [24]–[26]. Embedding-based metrics, including BERTScore, BLEURT, MoverScore, COMET, BARTScore, and MAUVE, improve semantic matching but still return scalar scores without exposing aligned information units or structured attribute disagreements [10], [12]–[15], [27]. Factuality-oriented evaluation emphasizes unsupported content, omissions, and consistency errors, but local auditability remains limited [1]–[3], [28]. RadOT-Eval follows this structured-evaluation view by comparing reference and candidate reports through explicit clinical units and their attributes, rather than through a single undifferentiated similarity score.

B. Radiology report generation as a case study

Radiology report generation has commonly been evaluated with metrics imported from machine translation, summarization, and image captioning [4], [29]–[31]. These generic metrics are simple to compute but were not designed for clinical factuality, finding omission, hallucination, or temporal-comparison errors [6], [8], [9], [24]. Clinical label and graph metrics address part of this gap. CheXpert and CheXbert map reports to observation labels, while RadGraph and RadGraph-XL extract radiology entities and relations for graph-based comparison [16]–[18], [32]. RadCliQ combines radiology-aware signals, including RadGraph-derived features, into a composite metric aligned with radiologist judgments [7]. These methods motivate the non-LLM baseline group in

our experiments; specifically, we compare against the official RadEvalX outputs for CheXbert, RadGraph-F1, and RadCliQ in Section V-B.

C. LLM-based radiology evaluators

Recent work has explored generative or learned clinical evaluation for radiology reports. GREEN-radllama2-7B introduces generative radiology report evaluation and error notation using a radiology-tuned language model to produce clinically significant error explanations and a scalar evaluation score [19]. RaTEScore similarly reflects the trend toward radiology-specific learned evaluation rather than generic text similarity alone [20]. These evaluators can provide clinically oriented judgments, but their decisions are not always decomposable into stable local alignment edges. Our goal is complementary: we evaluate whether structured evidence transport can achieve competitive cross-benchmark ranking while exposing unit-level alignments and monotone feature contributions.

D. Optimal transport for structured text comparison

Optimal transport provides a natural framework for comparing distributions or sets under a ground cost, with foundations in Earth-Mover-style distances and modern computational formulations [33]–[36]. Entropy regularization and Sinkhorn scaling make OT practical for repeated pairwise comparisons [37], [38]. Prior OT-based text metrics, such as Word Mover’s Distance and MoverScore, transport mass over words or contextual token representations to produce document-level similarity scores [13], [39]. RadOT-Eval differs in both support and objective: it transports mass over extracted clinical evidence units, uses a typed ground cost over stable clinical attributes, and then reads out clinically sensitive side-channel discrepancies under the resulting plan. Thus, OT is used not as a generic semantic distance, but as an auditable alignment layer for offline report-generation auditing. We also consider partial and unbalanced OT variants as ablations [40], [41].

III. PROBLEM AND DATA

A. Pair-level error prediction

In this radiology instantiation, each example consists of a reference report R and a candidate report C . The goal is to predict three human-annotated aggregate targets: total errors, clinically significant errors, and clinically insignificant errors. We treat these outputs as rank-oriented error-risk scores rather than calibrated absolute error-count estimates.

B. Benchmarks and preprocessing

ReXVal contains 200 report pairs from the Medical Information Mart for Intensive Care Chest X-ray (MIMIC-CXR) dataset, covering 50 studies with four retrieved candidate reports per study and radiologist error annotations [21], [42], [43]. It is used only for source-side fitting and selection. RadEvalX contains 100 Indiana University Chest X-ray (IU-Xray) reference reports paired with Memory-Driven Transformer (M2Tr)-generated candidates and expert error annotations; it is used only for final external evaluation [11], [30], [43], [44].

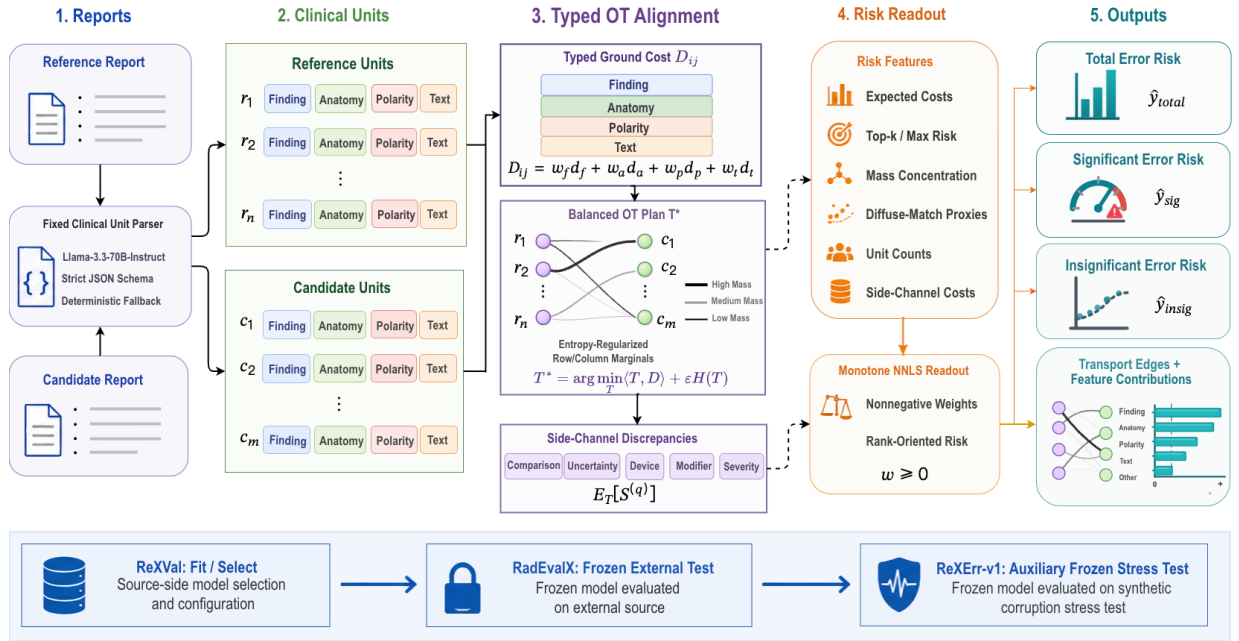


Fig. 1. Overview of RadOT-Eval. Reports are parsed into structured clinical units. Stable attributes define the OT ground cost and transport plan, while alignment-sensitive attributes are summarized as side-channel discrepancies. A monotone nonnegative readout combines alignment, discrepancy, concentration, diffuse-match, and unit-count features into rank-oriented error-risk scores.

TABLE I

BENCHMARKS, ROLES, AND CLINICAL-UNIT PREPROCESSING. UNIT AND FALLBACK COUNTS FOR REXVAL AND RAEVALX ARE REPORTED JOINTLY; REXERR-V1 IS USED ONLY FOR FROZEN BINARY STRESS TESTING.

Dataset	Pairs	Source	Role	Units	Fallback roles
ReXVal	200	MIMIC-CXR	Fit/select only	1,960	7
RadEvalX	100	IU-Xray	External test only		
ReXErr-v1	5,416	MIMIC-CXR	Frozen binary stress test only		

The official RadEvalX metric file provides per-pair scores for BLEU-4, BLEU-2, BERTScore, CheXbert, RadGraph-F1, and RadCliQ, enabling aligned baseline comparisons [7], [8], [10], [16], [17]. Together, these resources define the benchmark setting for our applied evaluation study and underscore the limited scale of expert-labeled evaluation resources in the medical domain.

In addition, we prepare ReXErr-v1 as an auxiliary synthetic binary stress test based on clinically meaningful synthetic report errors [22], [23]. We form 2,708 clean self-pairs and 2,708 error-injected pairs. Clean pairs receive zero synthetic error labels, while corrupted pairs contain sentence-level synthetic perturbations. We use ReXErr-v1 only to test whether the frozen evaluator assigns higher risk to corrupted reports than to clean self-pairs. We do not use its synthetic error counts or categories as fine-grained calibration targets because they are generated perturbation labels rather than radiologist-annotated report-level error burdens, and their severity distribution is not directly matched to the ReXVal or RadEvalX annotation schemes. Table I summarizes benchmark roles and clinical-unit preprocessing.

C. Clinical-unit extraction

Each report is converted into attribute-structured clinical units using a fixed Llama-3.3-70B-Instruct parser [45]. The prompt requests strict JSON with span text, canonical finding, surface finding, polarity, uncertainty, comparison, device, severity, anatomy, modifiers, and confidence fields. The schema is summarized in Appendix A-A; released repaired unit tables allow downstream reproduction without rerunning the 70B parser.

IV. RADOT-EVAL: STRUCTURED EVIDENCE TRANSPORT

RadOT-Eval is a structured evidence-alignment framework for paired documents that can be decomposed into domain-specific information units. In radiology report evaluation, these units are clinical statements with attributes such as finding, anatomy, polarity, uncertainty, comparison, device, modifier, and severity. The key technical design is to use OT only for auditable evidence alignment: stable attributes define the transport ground cost, while clinically sensitive attributes are withheld from matching and scored later as side-channel discrepancies. The method has three stages: unit extraction, auditable transport alignment, and monotone risk readout.

A. Attribute-structured clinical-unit alignment

For a pair of reports, optimal transport represents alignment as a nonnegative matrix T , where T_{ij} is the amount of mass assigned between reference unit r_i and candidate unit c_j . The transport plan is optimized with respect to a ground-cost matrix D , whose entry D_{ij} measures the mismatch between the two units. In RadOT-Eval, let $R = \{r_1, \dots, r_n\}$ and

$C = \{c_1, \dots, c_m\}$ denote the extracted reference and candidate clinical units. For each pair (r_i, c_j) , we compute attribute-specific alignment costs for finding, anatomy, polarity, and text:

$$D_{ij} = w_f d_{\text{find}}(r_i, c_j) + w_a d_{\text{anat}}(r_i, c_j) + w_p d_{\text{pol}}(r_i, c_j) + w_t d_{\text{text}}(r_i, c_j). \quad (1)$$

The weights are nonnegative and sum to one, i.e., $w_f, w_a, w_p, w_t \geq 0$ and $w_f + w_a + w_p + w_t = 1$. They control the relative emphasis placed on finding identity, anatomy, polarity, and lexical evidence when constructing the transport ground cost. In the method description, we treat these weights as predefined experimental design choices rather than learned pairwise matchers. The candidate weight priors and the final selected setting are specified in the source-only selection protocol in Section V-A.

Let $a_i = 1/n$ and $b_j = 1/m$. The primary RadOT-Eval system computes the entropy-regularized balanced transport plan [36], [37]

$$T^* = \arg \min_{T \in U(a,b)} \sum_{i,j} T_{ij} D_{ij} + \epsilon \sum_{i,j} T_{ij} (\log T_{ij} - 1), \quad (2)$$

where $U(a, b)$ enforces the row and column marginals. The entropy parameter ϵ controls alignment smoothness: smaller values produce sharper transport plans, while larger values distribute mass more diffusely across plausible matches. The candidate values and final selected value are reported with the source-only model-selection protocol in Section V-A.

B. Attribute-specific cost components

All attribute-specific component costs are normalized to $[0, 1]$, where 0 denotes agreement and larger values denote weaker alignment or stronger discrepancy. We use deterministic costs rather than learned pairwise matchers so that the transport plan remains auditable. Let $\tau(x)$ denote lower-cased alphanumeric tokenization of text field x , and let

$$J(A, B) = \begin{cases} 1, & A = B = \emptyset, \\ 0, & \mathbf{1}[A = \emptyset] + \mathbf{1}[B = \emptyset] = 1, \\ \frac{|A \cap B|}{|A \cup B|}, & \text{otherwise} \end{cases}$$

be the Jaccard similarity between token or label sets. Let \perp denote a missing categorical value and define $m_{\perp}(a, b) = \mathbf{1}[a = \perp] + \mathbf{1}[b = \perp]$. For categorical fields, we use

$$c_{\text{cat}}(a, b; \mu, \eta) = \begin{cases} 0, & a = b = \perp, \\ \mu, & m_{\perp}(a, b) = 1, \\ 0, & a = b, \\ \eta, & \text{otherwise,} \end{cases}$$

where μ is the missing-value penalty and η is the mismatch penalty. For set-valued label fields, after splitting normalized parser outputs on pipe, semicolon, or comma delimiters, define $m_{\emptyset}(A, B) = \mathbf{1}[A = \emptyset] + \mathbf{1}[B = \emptyset]$ and use

$$c_{\text{set}}(A, B; \mu) = \begin{cases} 0, & A = B = \emptyset, \\ \mu, & m_{\emptyset}(A, B) = 1, \\ 1 - J(A, B), & \text{otherwise.} \end{cases}$$

TABLE II
ALIGNMENT COSTS IN THE RADOT-EVAL GROUND COST. ALL COSTS ARE CLIPPED TO $[0, 1]$.

Component	Definition
Finding d_{find}	0 for exact nonempty canonical-finding match; otherwise $1 - J(\tau(x_r), \tau(x_c))$, where x concatenates canonical finding, surface finding, and span text.
Anatomy d_{anat}	$c_{\text{set}}(A_r, A_c; 0.6)$ over normalized anatomy-label sets.
Polarity d_{pol}	$c_{\text{cat}}(p_r, p_c; 0.5, 1.0)$ over normalized polarity labels.
Text d_{text}	$1 - J(\tau(s_r), \tau(s_c))$ over unit span texts.

Table II gives the exact alignment costs used in the transport ground cost. The finding cost first checks whether both units have the same nonempty canonical finding. If so, the cost is 0. Otherwise, it backs off to token overlap over the concatenation of canonical finding, surface finding, and unit span. This fallback makes the alignment less brittle when the parser normalizes semantically similar findings differently.

Side-channel costs use the same deterministic cost families but are not included in D_{ij} . Categorical side attributes, such as comparison, uncertainty, and device status, are measured with c_{cat} ; set-valued side attributes, such as modifier labels, are measured with c_{set} ; and severity is mapped to an ordinal scale before taking an absolute difference. These side-channel discrepancies are summarized under the transport plan for risk readout rather than used to determine the alignment itself. The exact side-channel constants and severity mapping used in the experiments are fixed before external evaluation and reported in the source-only experimental protocol in Section V-A. Their influence is audited in Section VI-C by removing severity and diffuse/concentration readout features.

This design avoids a common failure mode in structured report comparison. If every attribute is placed in the ground cost, the transport solver may avoid matching units that refer to the same clinical entity but disagree on an important side attribute. For example, a reference unit indicating that an opacity has improved and a candidate unit indicating that the same opacity is unchanged should still be aligned before the comparison discrepancy is scored. RadOT-Eval therefore uses stable attributes for alignment and reserves comparison, uncertainty, device, modifier, and severity for risk readout.

C. Monotone risk readout

The transport cost determines alignment, but not all clinically important attributes should determine matching. RadOT-Eval computes side-channel discrepancy matrices $S^{(q)}$ for comparison, uncertainty, device, modifier, and severity, then summarizes each by

$$\mathbb{E}_{T^*}[S^{(q)}] = \sum_{i,j} T_{ij}^* S_{ij}^{(q)}. \quad (3)$$

This design keeps alignment conservative while giving the readout access to clinically meaningful differences. Finding, anatomy, polarity, and text decide which units are comparable; comparison, uncertainty, device, modifier, and severity determine how much risk is associated with the aligned discrepancies.

The final feature vector contains expected alignment and side-channel costs, maximum and top- k costs, top- k mass-weighted risks, effective number of transport edges, top-mass concentration, transport entropy, diffuse-match proxies, and reference and candidate unit counts. Because the primary system uses balanced OT, all mass is transported; therefore, our “soft unmatched” features should not be interpreted as literal untransported mass. Instead, they measure whether the transported mass of a unit is concentrated on a single counterpart or diffusely spread across many weak matches. For each reference unit, define

$$\rho_i = \frac{\max_j T_{ij}^*}{a_i},$$

and for each candidate unit define

$$\gamma_j = \frac{\max_i T_{ij}^*}{b_j}.$$

Both quantities are clipped to $[0, 1]$. We compute reference and candidate diffuse-match masses as

$$M_R = \sum_i a_i(1 - \rho_i), \quad M_C = \sum_j b_j(1 - \gamma_j),$$

along with total and asymmetric summaries and low-confidence fractions

$$\frac{1}{n} \sum_i \mathbf{1}[\rho_i < \tau_{\text{diff}}], \quad \frac{1}{m} \sum_j \mathbf{1}[\gamma_j < \tau_{\text{diff}}].$$

We use $\tau_{\text{diff}} = 0.55$ as a fixed diffuse-match convention, chosen before external evaluation and not tuned on RadEvalX. These features act as soft omission and addition proxies under balanced transport: they are small when units have a dominant counterpart and larger when alignment mass is diffuse. The readout is monotone nonnegative least squares, so stronger discrepancy evidence cannot reduce predicted risk. This constraint also makes feature contributions interpretable after scaling.

D. Transport-constraint variants

The main system uses balanced OT. As ablations, we evaluate partial OT, which transports only a fraction of mass, and unbalanced OT, which relaxes marginal constraints with a mass-variation penalty [40], [41]. In partial OT, the plan satisfies

$$\begin{aligned} T\mathbf{1} &\leq a, \\ T^\top \mathbf{1} &\leq b, \\ \sum_{i,j} T_{ij} &= \tau, \quad 0 < \tau \leq 1, \end{aligned}$$

where τ is the transported mass. This allows a small amount of difficult mass to remain unmatched.

For unbalanced OT, we replace hard marginal equality with Kullback–Leibler (KL)-penalized marginal deviation:

$$\begin{aligned} T_{\text{UOT}}^* &= \arg \min_{T \geq 0} \sum_{i,j} T_{ij} D_{ij} + \epsilon \sum_{i,j} T_{ij} (\log T_{ij} - 1) \\ &\quad + \lambda_m \text{KL}(T\mathbf{1} \parallel a) + \lambda_m \text{KL}(T^\top \mathbf{1} \parallel b). \end{aligned}$$

Here the generalized KL divergence is

$$\text{KL}(u \parallel v) = \sum_i \left(u_i \log \frac{u_i}{v_i} - u_i + v_i \right).$$

The mass penalty λ_m controls how strongly the transported row and column masses must match the original unit masses. These variants use the same feature-generation and source-only selection principles. They are not used to replace the primary system; instead, they test whether relaxing balanced transport changes the trade-off across error severities.

V. EXPERIMENTAL PROTOCOL

A. Source-only model selection

All model-selection choices for RadOT-Eval are made using ReXVal only, including the transport-weight prior, entropy parameter, and readout configuration. For each predefined configuration, we run 5-fold GroupKFold by study and select the final system by macro held-out Spearman across the three targets. The selected model is frozen and evaluated once on RadEvalX, preventing target-benchmark label leakage.

The predefined alignment-prior grid varies the emphasis on finding identity, anatomy, polarity, and lexical evidence, including uniform, finding-heavy, anatomy-heavy, polarity-heavy, text-heavy, text-light, no-text, no-polarity, stable-prior, and parser-robust settings. The selected primary system uses the polarity-heavy ground-cost prior, $(w_f, w_a, w_p, w_t) = (0.250, 0.200, 0.400, 0.150)$, and entropy parameter $\epsilon = 0.20$. Side-channel constants are fixed before external evaluation rather than tuned on RadEvalX: comparison and uncertainty use $c_{\text{cat}}(\cdot, \cdot; 0.35, 1.0)$, device status uses $c_{\text{cat}}(\cdot, \cdot; 0.2, 1.0)$, and modifier labels use $c_{\text{set}}(\cdot, \cdot; 0.4)$. Severity is mapped to an ordinal scale, with none/normal = 0, mild = 0.33, moderate = 0.66, severe/marked = 1.0, empty = 0, and other nonempty unknown values = 0.5; severity discrepancy is the absolute difference between the two mapped values.

Appendix A-B reports the selected source-side configuration and additional full metrics.

Reproducibility controls. To support reproduction without rerunning the 70B parser, our reproducibility package includes repaired unit tables, feature matrices, selected configuration, fitted coefficients, prediction files, bootstrap outputs, ablation outputs, and evaluation scripts, subject to source-dataset data-use restrictions.

B. Baselines and statistics

The baselines cover standard automatic metrics, an open-source LLM-based evaluator, non-ensemble discrepancy models, and shortcut controls. For the official RadEvalX metrics, we use the distributed per-pair scores for BLEU-4, BLEU-2, BERTScore, CheXbert, RadGraph-F1, and RadCliQ [7], [8], [10], [16], [17]. Similarity scores are converted to risk by $1 - \text{score}$, while RadCliQ is already treated as an error-risk score.

For the LLM-based baseline, we use the Stanford AIMI GREEN model, StanfordAIMI/GREEN-RadLlama2-7b, through the

released `green_score`. GREEN inference wrapper with the model’s default reference-candidate report comparison prompt and output schema [19]. This checkpoint is a radiology-report evaluator fine-tuned from `StanfordAIMI/RadLLaMA-7b`. We run GREEN on the same 100 RadEvalX reference-candidate report pairs used for RadOT-Eval evaluation. We report two GREEN-derived signals because the released evaluator exposes both a scalar report-level GREEN score and structured error annotations. The scalar score is a quality-oriented score, so we convert it to an error-risk direction as $1 - \text{GREEN}$ and report this as GREEN risk. The native structured count is computed from GREEN’s six clinically significant error categories and is reported for total and clinically significant targets. We do not report a native GREEN count for clinically insignificant errors because the released GREEN schema does not provide a stable RadEvalX-style clinically insignificant error-count field.

The non-ensemble discrepancy baselines include text-only ridge, structured monotone, graph-derived monotone, and a graph neural network (GNN) discrepancy model. The shortcut controls compare full RadOT-Eval with a variant that removes the reference-unit count and with a reference-count-only model.

Spearman correlation is the primary metric because evaluators are often used to rank reports by clinical risk. Pearson, Kendall, MAE, and RMSE are reported in Appendix A-B. For clinically significant screening, we report AUROC, AUPRC, sensitivity at high-specificity operating points, and top-20% enrichment. Paired RadEvalX comparisons use bootstrap 95% confidence intervals for Spearman differences between RadOT-Eval and each comparator.

VI. RESULTS

A. Main RadEvalX transfer performance

The selected RadOT-Eval system obtains Spearman correlations of 0.715, 0.548, and 0.399 for total, clinically significant, and clinically insignificant errors, respectively. Individual bootstrap confidence intervals are $[0.594, 0.803]$, $[0.395, 0.677]$, and $[0.224, 0.559]$. Pearson, Kendall, and uncalibrated score-scale MAE/RMSE metrics are reported in Appendix A-B; Spearman correlation is the primary endpoint. Table III compares RadOT-Eval with official standard metrics, the open-source LLM-based evaluator baseline GREEN-radllama2-7B, non-ensemble discrepancy baselines, and shortcut controls.

Among official standard metrics, CheXbert is strongest for total and clinically significant errors, while RadCliQ is strongest for clinically insignificant errors. RadOT-Eval improves the corresponding point estimates by 0.224, 0.135, and 0.222 Spearman. Compared with GREEN risk, RadOT-Eval increases total, clinically significant, and clinically insignificant Spearman point estimates by 0.146, 0.115, and 0.258. Paired bootstrap intervals support reliable gains over several official standard metrics for total and clinically significant errors, while gains over the strongest baselines remain more

TABLE III
 RAEVALX SPEARMAN CORRELATIONS. OFFICIAL STANDARD METRICS USE DISTRIBUTED PER-PAIR SCORES. GREEN RISK DENOTES $1 - \text{GREEN}$ FROM THE RELEASED SCALAR GREEN SCORE, WHILE GREEN NATIVE COUNT DENOTES THE SUM OF GREEN’S NATIVE CLINICALLY SIGNIFICANT ERROR CATEGORIES. BOLD INDICATES THE BEST NON-DIAGNOSTIC EVALUATOR IN EACH COLUMN, WITH TIES BOLD; THE REFERENCE-COUNT-ONLY ROW IS A SHORTCUT DIAGNOSTIC, NOT A CLINICAL DISCREPANCY BASELINE.

System	Total	Sig.	Insig.
BLEU-4	0.108	0.096	0.046
BLEU-2	0.292	0.162	0.157
BERTScore	0.349	0.195	0.151
CheXbert	0.492	0.413	0.103
RadGraph-F1	0.285	0.159	0.147
RadCliQ	0.335	0.188	0.177
GREEN native count	0.296	0.382	–
GREEN risk	0.570	0.433	0.141
Text-only ridge	0.592	0.337	0.324
Structured monotone	0.612	0.398	0.256
Graph-derived monotone	0.569	0.469	0.206
GNN discrepancy model	0.607	0.398	0.119
Reference count only	0.474	0.201	0.410
RadOT-Eval w/o ref count	0.712	0.548	0.308
RadOT-Eval	0.715	0.548	0.399

uncertain on the 100-pair RadEvalX set. Detailed paired intervals are reported in Appendix A-C.

For clinically significant screening, RadOT-Eval improves AUROC/AUPRC from 0.696/0.745 for GREEN risk to 0.766/0.826, and improves sensitivity at 90% specificity from 0.161 to 0.403 (upper panel of Table IV).

B. Auxiliary ReXErr-v1 synthetic stress testing

Before applying RadOT-Eval to ReXErr-v1, we verify that the refit ReXVal readout exactly reproduces the selected RadEvalX predictions, with maximum absolute prediction differences below 10^{-14} . We then use ReXErr-v1 only as a frozen auxiliary binary corruption-sensitivity stress test. This experiment asks whether the selected evaluator assigns higher risk to synthetic error-injected reports than to clean self-pairs from the same source distribution; it is not used for model selection, hyperparameter tuning, or fine-grained error-type calibration.

The lower panel of Table IV shows the stress-test summary. A reference-count-only control obtains chance performance, indicating that the clean-versus-corrupted distinction is not explained by report complexity alone. Full RadOT-Eval separates clean from corrupted pairs with an AUROC of 0.768 and an AUPRC of 0.714. When each corrupted pair is compared with its clean counterpart from the same source report, RadOT-Eval assigns higher risk to the corrupted report in 99.0% of pairs. These results provide large-scale evidence that the frozen evaluator is sensitive to injected corruption, while the primary human-annotated evidence comes from ReXVal-only selection followed by frozen evaluation on the independent RadEvalX benchmark.

C. Ablation studies

Table V summarizes the architecture and transport-constraint ablations. Mean transport cost alone is weak, in-

TABLE IV

AUXILIARY BINARY EVALUATION. THE UPPER PANEL SCREENS FOR ANY CLINICALLY SIGNIFICANT ERROR ON RAdEVALX; THE LOWER PANEL TESTS FROZEN CLEAN-VERSUS-CORRUPTED SENSITIVITY ON REXERR-V1. SENS.@80/90 DENOTE SENSITIVITY AT 80%/90% SPECIFICITY; EXTRA REPORTS TOP-20% ENRICHMENT FOR RAdEVALX AND PAIRED WIN RATE FOR REXERR-V1.

Task	System	AUROC	AUPRC	Sens.@80	Sens.@90	Extra
RadEvalX sig. screen	GREEN native count	0.654	0.721	0.129	0.129	–
	GREEN risk	0.696	0.745	0.452	0.161	1.048
	RadOT-Eval	0.766	0.826	0.613	0.403	1.452
ReXErr-v1 corruption	Reference count only	0.500	0.500	–	–	–
	RadOT-Eval	0.768	0.714	–	–	0.990

TABLE V

ARCHITECTURE AND TRANSPORT-CONSTRAINT ABLATIONS. VARIANTS ARE SELECTED ON REXVAL AND EVALUATED ONCE ON RAdEVALX. BOLD MARKS THE BEST REPORTED ABLATION VALUE; THE PRIMARY RADOT-EVAL SYSTEM IS RETAINED FOR MAIN COMPARISONS BECAUSE IT IS STRONGEST FOR TOTAL AND CLINICALLY SIGNIFICANT ERRORS.

Variant	Macro	Total	Sig.	Insig.
Mean transport only	0.226	0.339	0.237	0.103
+ side-channel expected	0.398	0.561	0.479	0.154
+ top- k /max	0.429	0.629	0.518	0.141
+ learned cost weights	0.427	0.642	0.504	0.135
Full RadOT-Eval	0.554	0.715	0.548	0.399
Partial OT variant	0.519	0.641	0.464	0.453
Balanced OT variant	0.509	0.637	0.469	0.422
Unbalanced OT variant	0.504	0.684	0.406	0.422

dicating that report-level error risk is not captured by a single average alignment distance. Adding expected side-channel costs substantially improves total and clinically significant prediction. Top- k and maximum-risk features further improve high-severity rank. Within the feature-ablation block, the full feature set gives the largest gain for clinically insignificant errors, largely through unit-count and mass-distribution signals.

The transport-constraint ablation shows a severity-specific trade-off. Partial OT improves clinically insignificant ranking to 0.453, while the primary balanced RadOT-Eval remains strongest for total and clinically significant error prediction. Unbalanced OT improves total ranking among alternative variants but reduces clinically significant transfer.

All sensitivity variants in Table VI are selected or audited using ReXVal only and then evaluated frozen on RadEvalX. Performance is stable across nearby entropy values, transport-weight priors, and readout-feature audits. Although some nearby settings have slightly higher RadEvalX point estimates, they are not selected because the final configuration is chosen only by source-side ReXVal GroupKFold performance. Removing severity features or diffuse/concentration features also preserves the main conclusions, suggesting that the reported transfer performance is not driven by a single hand-specified severity mapping or diffuse-match threshold.

D. Shortcut, robustness, and interpretability analyses

Because the feature-importance analysis assigns high weight to reference-unit count for clinically insignificant errors, we perform shortcut audits. Table VII shows that total and clinically significant prediction are not explained by reference complexity: removing reference-unit count preserves total and

TABLE VI

SENSITIVITY ANALYSIS FOR TRANSPORT AND READOUT CHOICES. THE BOLD ROW IS THE REXVAL-SELECTED PRIMARY SYSTEM, NOT THE HIGHEST RAdEVALX POINT ESTIMATE. FEAT. DENOTES THE NUMBER OF READOUT FEATURES; SIG./INSIG. DENOTES CLINICALLY SIGNIFICANT/CLINICALLY INSIGNIFICANT SPEARMAN CORRELATIONS.

Variant	ϵ	Feat.	ReXVal	RadEvalX	Total	Sig./Insig.
Selected full model	0.20	66	0.846	0.554	0.715	0.548 / 0.399
$\epsilon = 0.05$	0.05	66	0.846	0.563	0.726	0.542 / 0.423
$\epsilon = 0.10$	0.10	66	0.844	0.565	0.734	0.558 / 0.404
Uniform weights	0.20	66	0.845	0.554	0.708	0.548 / 0.405
Text-light weights	0.20	66	0.839	0.562	0.722	0.565 / 0.400
No text cost	0.20	66	0.838	0.561	0.724	0.555 / 0.404
No polarity cost	0.20	66	0.839	0.546	0.709	0.535 / 0.396
No severity features	0.20	61	0.851	0.551	0.710	0.556 / 0.387
No diffuse features	0.20	49	0.845	0.558	0.709	0.556 / 0.409

TABLE VII

SHORTCUT AND ROBUSTNESS DIAGNOSTICS. PARTIAL CORRELATIONS ARE RANK RESIDUAL CORRELATIONS AFTER CONTROLLING FOR REFERENCE-UNIT COUNT.

Diagnostic	Total	Sig.	Insig.
Full RadOT-Eval	0.715	0.548	0.399
RadOT-Eval without ref count	0.712	0.548	0.308
Reference count only	0.474	0.201	0.410
Partial corr. controlling ref count	0.613	0.529	0.077
Without fallback pairs	0.708	0.535	0.391
10% unit dropout	0.674	0.516	0.349
25% unit dropout	0.588	0.469	0.264

clinically significant correlations at 0.712 and 0.548, while reference-count only is much weaker. By contrast, clinically insignificant errors are strongly complexity-driven: reference-count only reaches 0.410, and the partial correlation after controlling for reference count drops to 0.077. This pattern is an important severity-specific property of the target rather than only a model artifact.

Parser robustness is stable. Removing all three RadEvalX pairs affected by sentence fallback preserves the main conclusions: the total, clinically significant, and clinically insignificant Spearman correlations become 0.708, 0.535, and 0.391, respectively. Under random clinical-unit dropout, performance degrades smoothly; at 10% unit dropout, the total and clinically significant Spearman correlations remain 0.674 and 0.516, and at 25% dropout they remain 0.588 and 0.469.

Error-type analysis supports semantic interpretability (Table VIII). Significant finding omissions are associated with side-channel maximum risk, top-risk summaries, and side-channel expected sums, with Spearman values up to 0.542. Significant comparison omissions align with comparison expected cost, with Spearman 0.501. Uncertainty omissions align with uncertainty features, although this category is rare in RadEvalX and should be interpreted cautiously. Risk-bucket analysis also shows monotonic stratification: from the lowest to highest predicted quintile, mean true total errors increase from 0.70 to 5.05, clinically significant errors from 0.20 to 2.85, and clinically insignificant errors from 0.45 to 1.90.

Qualitative transport reconstructions show that high clinically significant cases are driven by edges involving missed opacity, pleural-effusion, comparison, or modifier content, while high clinically insignificant cases show multiple moderate mismatches and stronger unit-count or mass-

TABLE VIII
REPRESENTATIVE RadevalX ERROR-TYPE ALIGNMENT. LOW-COUNT
CATEGORIES ARE EXPLORATORY.

Severity / category	Best aligned feature	Nonzero	Spearman
Sig. finding omission	Side maximum sum	56	0.542
Sig. finding omission	Top-risk sum	56	0.525
Sig. comparison omission	Comparison expected	14	0.501
Sig. uncertainty omission	Uncertainty expected	2	0.433
Insig. finding omission	Reference unit count	43	0.438
Insig. comparison omission	Comparison top-3 mean	7	0.317

distribution contributions. Representative transport-edge and feature-contribution tables are provided in Appendix A-D.

VII. DISCUSSION AND LIMITATIONS

The results support treating high-stakes generated-text evaluation as structured clinical-unit comparison rather than only scalar similarity estimation. RadOT-Eval uses OT as an auditable alignment layer, not as a claim of a new OT solver. The technical novelty is the domain-specific OT formulation: transport is performed over attribute-structured clinical units, the ground cost is restricted to stable alignment anchors, and clinically sensitive attributes are scored only after alignment as side-channel risk evidence. Because all choices are selected on ReXVal and frozen before RadEvalX evaluation, the transfer results are less likely to reflect target-benchmark tuning. RadOT-Eval yields higher point estimates than the official RadEvalX metrics and GREEN-radllama2-7B on all three ranking targets, although intervals against the strongest baselines remain uncertain on the 100-pair external set. The readout should be interpreted as a rank-oriented risk score, not a calibrated error-count estimator.

The ablations clarify why structured evidence transport is useful. Mean transport cost alone is weak, indicating that report-level risk is not captured by a single average alignment distance. Side-channel discrepancies and top- k risk summaries are important for high-severity errors, while unit-count and mass-distribution features explain part of the low-severity target. This supports the design choice to separate stable alignment dimensions from risk readout channels: findings, anatomy, polarity, and lexical evidence define which units are comparable, while comparison, uncertainty, device, modifier, and severity discrepancies are scored under the resulting transport plan. The analyses also reveal a severity-specific structure. Total and clinically significant prediction remain strong after controlling for reference complexity, whereas clinically insignificant prediction is more strongly associated with report complexity and cumulative mild mismatch burden.

The ReXErr-v1 experiment should be interpreted only as an auxiliary binary corruption-sensitivity stress test, not as a fine-grained external validation benchmark. It shows that the frozen evaluator is sensitive to injected corruptions in paired source-controlled comparisons, but the primary external evidence remains the human-annotated RadEvalX benchmark. Several limitations remain. The main external benchmark contains only 100 pairs, which widens paired uncertainty intervals against strong baselines. RadOT-Eval also

depends on clinical-unit extraction from a large local instruction model, making raw-text re-extraction more expensive than the downstream transport and readout stages. The official GREEN-radllama2-7B comparison uses the released six-category schema, which does not provide a stable RadEvalX-style clinically insignificant count field. Finally, this paper studies a single non-ensemble evaluator without target-domain adaptation or joint parser training. Future work should study larger external benchmarks, improved anatomical and laterality normalization, calibrated count prediction, and sentence-level error localization. RadOT-Eval should be used as a rank-oriented audit signal for model development and targeted error analysis, not as an autonomous clinical decision tool.

VIII. CONCLUSION

We presented RadOT-Eval, a structured evidence-transport framework for auditable radiology report evaluation. The problem is to predict clinically meaningful report-level discrepancies that may be missed by scalar lexical, semantic, or label-overlap metrics. RadOT-Eval addresses this problem by decomposing reference and candidate reports into attribute-structured clinical units, aligning stable evidence with entropy-regularized OT, and reading out clinically relevant side-channel discrepancies through a monotone risk model. Under ReXVal-only selection and frozen RadEvalX evaluation, RadOT-Eval achieves strong ranking performance for total and clinically significant errors and remains competitive with official standard metrics and the open-source LLM-based evaluator baseline. The results suggest that structured evidence transport is a practical audit layer for model-development workflows in high-stakes generated clinical text, provided that model-selection choices are fixed before external testing.

ACKNOWLEDGMENT

This research was, in part, funded by the Advanced Research Projects Agency for Health (ARPA-H). The views and conclusions contained in this document are those of the authors and should not be interpreted as representing the official policies, either expressed or implied, of the United States Government.

APPENDIX A ADDITIONAL RESULTS

- A. *Parser Schema and Category Definitions*
- B. *Source-Side Selection and Full Metrics*
- C. *Paired Statistical Tests*
- D. *Qualitative Reconstructions*

REFERENCES

- [1] J. Maynez, S. Narayan, B. Bohnet, and R. McDonald, "On faithfulness and factuality in abstractive summarization," in *Proceedings of the 58th Annual Meeting of the Association for Computational Linguistics*, 2020, pp. 1906–1919.
- [2] W. Kryściński, B. McCann, C. Xiong, and R. Socher, "Evaluating the factual consistency of abstractive text summarization," in *Proceedings of the 2020 Conference on Empirical Methods in Natural Language Processing*, 2020, pp. 9332–9346.

TABLE IX
PARSER SCHEMA AND RAdEVALX ERROR-CATEGORY DEFINITIONS.

Clinical-unit schema	
span_text	Verbatim report span supporting the unit
canonical_finding	Normalized finding label for alignment
surface_finding	Finding phrase as expressed in text
polarity	Assertion status, e.g., present, absent, uncertain
uncertainty	Certainty status, e.g., definite, probable, possible
comparison	Temporal comparison, e.g., stable, improved, worsened
device	Canonical device label or null
attributes.severity	Free-text severity normalized downstream
anatomy	Canonical anatomy labels with surface phrases
modifiers	Canonical modifier labels with surface phrases
confidence	Parser confidence; fallback units use 0.50

RadEvalX error categories	
1	False prediction of finding
2	Omission of finding
3	Incorrect location or position of finding
4	Incorrect severity of finding
5	Unsupported mention of comparison
6	Omission of comparison with previous study
7	Unsupported mention of uncertainty
8	Omission of uncertainty present in reference

TABLE X
SOURCE-SIDE SELECTION AND FULL RAdEVALX METRICS. BOLD INDICATES THE SELECTED SOURCE-SIDE CONFIGURATION.

ReXVal GroupKFold selection				
Ground cost	ϵ	Macro	Total	Sig./Insig.
Polarity-heavy	0.20	0.846	0.900	0.842 / 0.797
Text-heavy	0.20	0.846	0.897	0.846 / 0.794
Polarity-heavy	0.05	0.846	0.899	0.844 / 0.794
Uniform-basic	0.20	0.845	0.899	0.844 / 0.792
Finding-heavy	0.05	0.845	0.898	0.844 / 0.793

Full RadEvalX metrics for selected RadOT-Eval				
Target	MAE	RMSE	Pearson	Spearman / Kendall
Total	11.692	12.122	0.713	0.715 / 0.556
Significant	6.786	7.350	0.524	0.548 / 0.421
Insignificant	5.085	5.274	0.439	0.399 / 0.310

TABLE XI
PAIRED BOOTSTRAP CONFIDENCE INTERVALS AGAINST OFFICIAL RAdEVALX STANDARD METRICS. $\Delta\rho$ IS RADOT-EVAL MINUS COMPARATOR.

Target	Comparator	ρ_c	$\Delta\rho$	95% CI
Total	BERTScore	0.349	0.366	[0.179,0.556]
Total	BLEU-2	0.292	0.424	[0.224,0.624]
Total	BLEU-4	0.108	0.608	[0.370,0.833]
Total	CheXbert	0.492	0.224	[0.052,0.406]
Total	RadCliQ	0.335	0.381	[0.203,0.567]
Total	RadGraph-F1	0.285	0.431	[0.241,0.617]
Sig.	BERTScore	0.195	0.353	[0.151,0.549]
Sig.	BLEU-2	0.162	0.386	[0.169,0.608]
Sig.	BLEU-4	0.096	0.452	[0.213,0.677]
Sig.	CheXbert	0.413	0.135	[-0.064,0.326]
Sig.	RadCliQ	0.188	0.360	[0.162,0.548]
Sig.	RadGraph-F1	0.159	0.389	[0.187,0.600]
Insig.	BLEU-4	0.046	0.352	[0.109,0.593]
Insig.	CheXbert	0.103	0.296	[0.076,0.523]
Insig.	RadCliQ	0.177	0.222	[0.031,0.409]

- [3] A. Pagnoni, V. Balachandran, and Y. Tsvetkov, "Understanding factuality in abstractive summarization with FRANK: A benchmark for factuality metrics," in *Proceedings of the 2021 Conference of the North American Chapter of the Association for Computational Linguistics: Human Language Technologies*, 2021, pp. 4812–4829.
- [4] B. Jing, P. Xie, and E. P. Xing, "On the automatic generation of medical imaging reports," in *Proceedings of the 56th Annual Meeting of the Association for Computational Linguistics*, 2018, pp. 2577–2586.
- [5] G. Liu, T.-M. H. Hsu, M. McDermott, W. Boag, W.-H. Weng, P. Szolovits, and M. Ghassemi, "Clinically accurate chest x-ray report generation," in *Proceedings of Machine Learning Research*, vol. 106, 2019, pp. 249–269.
- [6] Y. Miura, Y. Zhang, E. Tsai, C. Langlotz, and D. Jurafsky, "Improving factual completeness and consistency of image-to-text radiology report generation," in *Proceedings of the 2021 Conference of the North American Chapter of the Association for Computational Linguistics: Human Language Technologies*, 2021, pp. 5288–5304.
- [7] F. Yu, M. Endo, R. Krishnan, I. Pan, A. Tsai, E. P. Reis, E. K. U. N. Fonseca, H. M. H. Lee, Z. S. H. Abad, A. Y. Ng, C. P. Langlotz, V. K. Venugopal, and P. Rajpurkar, "Evaluating progress in automatic chest x-ray radiology report generation," *Patterns*, vol. 4, no. 9, p. 100802, 2023.
- [8] K. Papineni, S. Roukos, T. Ward, and W.-J. Zhu, "BLEU: a method for automatic evaluation of machine translation," in *Proceedings of the 40th Annual Meeting of the Association for Computational Linguistics*, 2002, pp. 311–318.
- [9] C.-Y. Lin, "ROUGE: A package for automatic evaluation of summaries," in *Text Summarization Branches Out*, 2004, pp. 74–81.
- [10] T. Zhang, V. Kishore, F. Wu, K. Q. Weinberger, and Y. Artzi, "BERTScore: Evaluating text generation with BERT," in *International Conference on Learning Representations*, 2020.
- [11] A. R. Calamida, F. Nooralhazadeh, M. Rohanian, M. Nishio, K. Fujimoto, and M. Krauthammer, "Radiology Report Generation Models Evaluation Dataset For Chest X-rays (RadEvalX)," *PhysioNet*, 2024, version 1.0.0.
- [12] T. Sellam, D. Das, and A. P. Parikh, "BLEURT: Learning robust metrics for text generation," in *Proceedings of the 58th Annual Meeting of the Association for Computational Linguistics*, 2020, pp. 7881–7892.
- [13] W. Zhao, M. Peyrard, F. Liu, Y. Gao, C. M. Meyer, and S. Eger, "MoverScore: Text generation evaluating with contextualized embeddings and earth mover distance," in *Proceedings of the 2019 Conference on Empirical Methods in Natural Language Processing and the 9th International Joint Conference on Natural Language Processing*, 2019, pp. 563–578.
- [14] R. Rei, C. Stewart, A. C. Farinha, and A. Lavie, "COMET: A neural framework for MT evaluation," in *Proceedings of the 2020 Conference on Empirical Methods in Natural Language Processing*, 2020, pp. 2685–2702.
- [15] W. Yuan, G. Neubig, and P. Liu, "BARTScore: Evaluating generated text as text generation," in *Advances in Neural Information Processing Systems*, vol. 34, 2021, pp. 27 263–27 277.
- [16] A. Smit, S. Jain, P. Rajpurkar, A. Pareek, A. Y. Ng, and M. P. Lungren, "Combining automatic labelers and expert annotations for accurate radiology report labeling using BERT," in *Proceedings of the 2020 Conference on Empirical Methods in Natural Language Processing*, 2020, pp. 1500–1519.
- [17] S. Jain, A. Agrawal, A. Saporta, S. Q. H. Truong, D. N. Duong, T. Bui, P. Chambon, Y. Zhang, M. P. Lungren, A. Y. Ng, C. P. Langlotz, and P. Rajpurkar, "RadGraph: Extracting clinical entities and relations from radiology reports," in *Proceedings of the Neural Information Processing Systems Track on Datasets and Benchmarks*, vol. 1, 2021.
- [18] J.-B. Delbrouck, P. Chambon, Z. Chen, M. Varma, A. Johnston, L. Blankemeier, D. Van Veen, T. Bui, S. Truong, and C. Langlotz, "RadGraph-XL: A large-scale expert-annotated dataset for entity and relation extraction from radiology reports," in *Findings of the Association for Computational Linguistics: ACL 2024*, 2024, pp. 12 902–12 915.
- [19] S. Ostmeier, J. Xu, Z. Chen, M. Varma, L. Blankemeier, C. Bluethgen, A. E. Michalson, M. Moseley, C. Langlotz, A. S. Chaudhari, and J.-B. Delbrouck, "GREEN: Generative radiology report evaluation and error notation," in *Findings of the Association for Computational Linguistics: EMNLP 2024*, 2024, pp. 374–390.
- [20] W. Zhao, C. Wu, X. Zhang, Y. Zhang, Y. Wang, and W. Xie, "RaTEScore: A metric for radiology report generation," in *Proceedings*

TABLE XII

REPRESENTATIVE HIGH-RISK TRANSPORT EDGES FROM QUALITATIVE RECONSTRUCTIONS. MW DENOTES MASS-WEIGHTED; EDGES ARE SELECTED FOR EXPLANATION ONLY AND ARE NOT USED FOR MODEL SELECTION.

Case	Rank	Reference unit	Candidate unit	Mass	Align	Side	MW risk
report699	1	opacity on the lateral view over the heart, present on previous exam, suggesting chronic subsegmental atelectasis or scarring	heart and cardiomeastinal silhouette are normal in size and contour	0.119	0.476	3.0	0.413
report699	2	opacity on the lateral view over the heart, present on previous exam, suggesting chronic subsegmental atelectasis or scarring	osseous structures are intact	0.100	0.586	3.0	0.359
report699	3	no definite pleural effusion seen	there is no focal air space pleural or pneumothorax	0.239	0.448	1.0	0.346
report1860	1	no focal airspace opacity	apparent interval increase in low density at the left <unk>	0.050	0.550	3.0	0.176
report1860	2	lungs are clear	apparent interval increase in low density at the left <unk>	0.067	0.400	2.0	0.160
report1860	3	levocurvature of the lumbar spine with significant degenerative change	apparent interval increase in low density at the left <unk>	0.033	0.584	4.0	0.151

TABLE XIII

REPRESENTATIVE FEATURE CONTRIBUTIONS FROM QUALITATIVE CASES. CONTRIBUTIONS ARE APPROXIMATE SCALED MONOTONE NONNEGATIVE LEAST-SQUARES (NNLS) TERMS.

Case/target	Feature	Coeff.	Contribution
report699 total	Modifier expected	7.224	4.770
report699 total	Comparison top-3 MW	3.534	3.534
report699 total	Effective edges	19.877	3.019
report699 sig.	Modifier expected	6.824	4.505
report699 sig.	Comparison top-3 MW	3.404	3.404
report1860 insig.	Reference unit count	3.972	3.404
report1860 insig.	Anatomy expected	1.496	0.980
report1860 insig.	Effective edges	2.630	0.920

of the 2024 Conference on Empirical Methods in Natural Language Processing, 2024, pp. 15004–15019.

- [21] F. Yu, M. Endo, R. Krishnan, I. Pan, A. Tsai, E. P. Reis, E. Kaiser Ururahy Nunes Fonseca, H. Lee, Z. Shakeri, A. Ng, C. Langlotz, V. K. Venugopal, and P. Rajpurkar, “Radiology Report Expert Evaluation (ReXVal) Dataset,” *PhysioNet*, 2023, version 1.0.0.
- [22] V. M. Rao, S. Zhang, J. N. Acosta, S. Adithan, and P. Rajpurkar, “ReX-Err: Synthesizing clinically meaningful errors in diagnostic radiology reports,” *arXiv preprint arXiv:2409.10829*, 2024.
- [23] V. Rao, S. Zhang, J. Acosta, S. Adithan, and P. Rajpurkar, “ReXErr-v1: Clinically meaningful chest x-ray report errors derived from MIMIC-CXR,” *PhysioNet*, 2025, version 1.0.0.
- [24] S. Banerjee and A. Lavie, “METEOR: An automatic metric for MT evaluation with improved correlation with human judgments,” in *Proceedings of the ACL Workshop on Intrinsic and Extrinsic Evaluation Measures for Machine Translation and/or Summarization*, 2005, pp. 65–72.
- [25] R. Vedantam, C. L. Zitnick, and D. Parikh, “CIDEr: Consensus-based image description evaluation,” in *Proceedings of the IEEE Conference on Computer Vision and Pattern Recognition*, 2015, pp. 4566–4575.
- [26] P. Anderson, B. Fernando, M. Johnson, and S. Gould, “SPICE: Semantic propositional image caption evaluation,” in *Computer Vision – ECCV 2016*, 2016, pp. 382–398.
- [27] K. Pillutla, S. Swayamdipta, R. Zellers, J. Thickstun, S. Welleck, Y. Choi, and Z. Harchaoui, “MAUVE: Measuring the gap between neural text and human text using divergence frontiers,” in *Advances in Neural Information Processing Systems*, vol. 34, 2021, pp. 4816–4828.
- [28] T. Scialom, P.-A. Dray, S. Lamprier, B. Piwowarski, J. Staiano, A. Wang, and P. Gallinari, “QuestEval: Summarization asks for fact-based evaluation,” in *Proceedings of the 2021 Conference on Empirical Methods in Natural Language Processing*, 2021, pp. 6594–6604.
- [29] X. Wang, Y. Peng, L. Lu, Z. Lu, and R. M. Summers, “TieNet: Text-image embedding network for common thorax disease classification and reporting in chest x-rays,” in *Proceedings of the IEEE Conference on Computer Vision and Pattern Recognition*, 2018, pp. 9049–9058.
- [30] Z. Chen, Y. Song, T.-H. Chang, and X. Wan, “Generating radiology reports via memory-driven transformer,” in *Proceedings of the 2020 Conference on Empirical Methods in Natural Language Processing*, 2020, pp. 1439–1449.
- [31] Z. Chen, Y. Shen, Y. Song, and X. Wan, “Cross-modal memory networks for radiology report generation,” in *Proceedings of the 59th Annual Meeting of the Association for Computational Linguistics and the 11th International Joint Conference on Natural Language Processing*, 2021, pp. 5904–5914.
- [32] J. Irvin, P. Rajpurkar, M. Ko, Y. Yu, S. Ciurea-Ilcus, C. Chute, H. Marklund, B. Haghgoo, R. Ball, K. Shpanskaya, J. Seekins, D. A. Mong, S. S. Halabi, J. K. Sandberg, R. Jones, D. B. Larson, C. P. Langlotz, B. N. Patel, M. P. Lungren, and A. Y. Ng, “CheXpert: A large chest radiograph dataset with uncertainty labels and expert comparison,” in *Proceedings of the AAAI Conference on Artificial Intelligence*, vol. 33, no. 1, 2019, pp. 590–597.
- [33] Y. Rubner, C. Tomasi, and L. J. Guibas, “The earth mover’s distance as a metric for image retrieval,” *International Journal of Computer Vision*, vol. 40, no. 2, pp. 99–121, 2000.
- [34] C. Villani, *Optimal Transport: Old and New*. Springer, 2009.
- [35] F. Santambrogio, *Optimal Transport for Applied Mathematicians*. Birkhäuser, 2015.
- [36] G. Peyré and M. Cuturi, “Computational optimal transport,” *Foundations and Trends in Machine Learning*, vol. 11, no. 5–6, pp. 355–607, 2019.
- [37] M. Cuturi, “Sinkhorn distances: Lightspeed computation of optimal transport,” in *Advances in Neural Information Processing Systems*, vol. 26, 2013, pp. 2292–2300.
- [38] J. Altschuler, J. Weed, and P. Rigollet, “Near-linear time approximation algorithms for optimal transport via sinkhorn iteration,” in *Advances in Neural Information Processing Systems*, vol. 30, 2017.
- [39] M. J. Kusner, Y. Sun, N. I. Kolkin, and K. Q. Weinberger, “From word embeddings to document distances,” in *Proceedings of the 32nd International Conference on Machine Learning*, vol. 37, 2015, pp. 957–966.
- [40] A. Figalli, “The optimal partial transport problem,” *Archive for Rational Mechanics and Analysis*, vol. 195, no. 2, pp. 533–560, 2010.
- [41] L. Chizat, G. Peyré, B. Schmitzer, and F.-X. Vialard, “Scaling algorithms for unbalanced transport problems,” *Mathematics of Computation*, vol. 87, no. 314, pp. 2563–2609, 2018.
- [42] A. E. W. Johnson, T. J. Pollard, S. J. Berkowitz, N. R. Greenbaum, M. P. Lungren, C.-y. Deng, R. G. Mark, and S. Horng, “MIMIC-CXR, a de-identified publicly available database of chest radiographs with free-text reports,” *Scientific Data*, vol. 6, no. 317, 2019.
- [43] A. L. Goldberger, L. A. N. Amaral, L. Glass, J. M. Hausdorff, P. C. Ivanov, R. G. Mark, J. E. Mietus, G. B. Moody, C.-K. Peng, and H. E. Stanley, “Physiobank, physiotookit, and physionet: Components of a new research resource for complex physiologic signals,” *Circulation*, vol. 101, no. 23, pp. e215–e220, 2000.
- [44] D. Demner-Fushman, M. D. Kohli, M. B. Rosenman, S. E. Shooshan, L. Rodriguez, S. Antani, G. R. Thoma, and C. J. McDonald, “Preparing a collection of radiology examinations for distribution and retrieval,” *Journal of the American Medical Informatics Association*, vol. 23, no. 2, pp. 304–310, 2016.
- [45] A. Grattafiori et al., “The Llama 3 herd of models,” *arXiv preprint arXiv:2407.21783*, 2024.